DOI: 10.1002/ejic.200600786

Competing Radical and Non-Radical Pathways for the Decomposition of $LFe^{II}(H_2O_2)$ Complexes: a Density Functional Study

Anna E. Anastasi,[a] Achim Lienke,[b] Peter Comba,[c] Heidi Rohwer,[c] and John E. McGrady*[d]

Keywords: Density functional calculations / Oxido ligands / O–O activation / Electronic structure / Transition states

Density functional theory has been used to explore the mechanism of hydrogen peroxide decomposition when coordinated to a bispidone iron(II) complex. Two quite distinct pathways are identified, one involving O–O bond homolysis followed by a "rebound" hydrogen atom abstraction, the other involving proton transfer followed by O–O bond heterolysis. A water molecule in the second coordination sphere plays a key role in both pathways.

Introduction

Mononuclear non-heme iron enzymes are involved in many different types of biological oxidation reactions, including hydroxylation and hydroperoxidation of C–H bonds, cleavage of aromatic rings and oxidative ring closure.[1–3] As a result, there has been a great deal of interest in synthesising model complexes that mimic aspects of the structure and reactivity of these enzymes. The chemistry of model complexes with multidentate nitrogen-donor ligands such as N4Py,[4] trispicene[5] and the pentadentate N_2Py_3 bispidones,[6] L^1 and L^2 (Scheme 1) is particularly well developed. The Fe^{II} complexes are known to be potent bleaching catalysts,[7] reacting with excess H_2O_2 to form hydroperoxide species, $LFe^{III}(OOH)$,[4–6,8] which then generate $LFe^{IV}(O)$ by homolytic cleavage of the O–O bond.[9] Whilst the mechanism of decomposition of the $LFe^{III}(OOH)$ species has been extensively explored by both experiment and theory, the initial formation of the Fe^{III} species has received comparatively little attention. There are, however, obvious parallels with classic Fenton chemistry, where H_2O_2 is used to oxidise aqueous solutions of Fe^{II}, eventually yielding Fe^{III} if no substrate is present.[10] Although the Fenton reagent has been used extensively in organic chemistry for over a century, the precise identity of the active intermediate remains a topic of debate.[11] The Haber–Weiss mechanism,[12,13] first proposed in 1934, identifies OH radicals as the active oxidant, a suggestion that has been substantiated by radical trapping experiments and also kinetic comparisons with radiolytically generated radicals. Alternatively, the reactive species may be a high-valent iron complex such as $Fe^{IV}(O)$ as first suggested by Bray and Gorin in 1932.[14] The participation of high-valent oxido–iron species has been supported by a detailed kinetic analysis by Kremer,[15] which suggested that the Fe^{III} products were formed by comproportionation of an intermediate $Fe^{IV}(O)$ species with excess Fe^{II}.

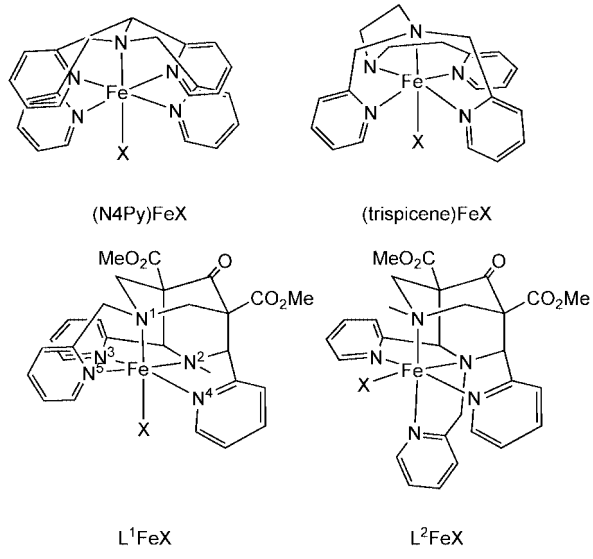

Scheme 1. Structure of complexes of pentadentate ligands, N4Py, trispicene and the bispidones L^1 and L^2.

[a] Department of Chemistry, University of York, Heslington, York, YO10 5DD, United Kingdom
Fax: +44-1904-432516
E-mail: aa155@york.ac.uk
[b] Unilever Research and Development, Olivier van Noortlaan 120, 3133AT Vlaadingen, The Netherlands
Fax: +31-10-460-5166
E-mail: achim.lienke@unilever.com
[c] Universität Heidelberg, Anorganisch-Chemisches Institut, Im Neuenheimer Feld 270, 69120 Heidelberg, Germany
Fax: +49-6226-546617
E-mail: comba@aci.uni-heidelberg.de
[d] WestCHEM, Department of Chemistry, University of Glasgow, Glasgow, G12 8QQ, United Kingdom
Fax: +44-141-3304888
E-mail: j.mcgrady@chem.gla.ac.uk

Buda et al. have recently used density functional theory to explore the energetics of the reaction between aqueous Fe^{II} and H_2O_2.[16,17] The first step in their proposed reaction pathway (Scheme 2) involves a ligand-substitution reaction where H_2O_2 replaces a molecule of water in the first coordination sphere of $[Fe(H_2O)_6]^{2+}$, giving $[(H_2O)_5Fe^{II}(H_2O_2)]^{2+}$. Meyerstein and co-workers have argued that coordination of the H_2O_2 is a necessary precursor to bond cleavage, as the alternative, outer-sphere electron transfer, is energetically unfavourable.[11d,18] Homolytic cleavage of the O–O bond then leads directly to an Fe^{IV} species, $[(H_2O)_4Fe^{IV}(OH)_2]^{2+}$, which subsequently rearranges by proton-transfer to the product, $[Fe^{IV}(H_2O)_5(O)]^{2+}$. A critical feature of the pathway is that as the O–O bond elongates, the developing OH radical abstracts a hydrogen atom from a neighbouring water ligand, and so is effectively trapped in the first coordination sphere. Thus, although the O–O bond cleavage is homolytic, no free radicals are released into solution. The putative $Fe^{IV}(O)$ intermediate in Scheme 2, $[(H_2O)_5Fe^{IV}(O)]^{2+}$, has recently been obtained by oxidation of aqueous Fe^{II} with ozone, and characterised using a combination of Mössbauer and X-ray absorption spectroscopy.[19] Consistent with Kremer's scheme, this species does indeed comproportionate with excess $[Fe^{II}(H_2O)_6]^{2+}$ to form an Fe^{III} dimer $[(H_2O)_4Fe^{III}(OH)_2Fe^{III}(H_2O)_4]^{4+}$. The latter is *not*, however, observed when H_2O_2 is used in place of O_3, suggesting that $[(H_2O)_5Fe^{IV}(O)]^{2+}$ is not the active Fenton intermediate, at least in aqueous solution.

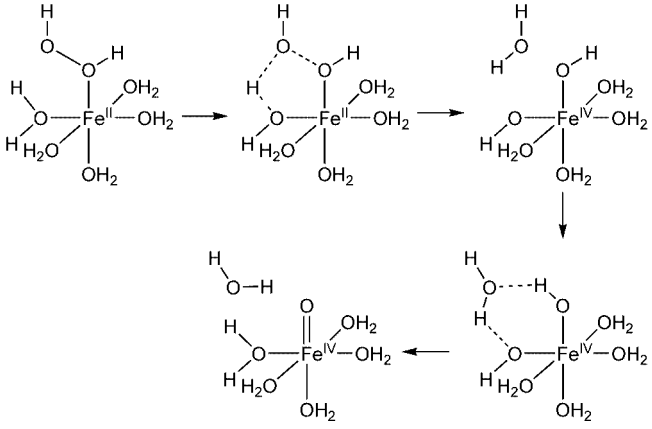

Scheme 2. Mechanism for the decomposition of $[Fe^{II}(H_2O)_5(H_2O_2)]^{2+}$ proposed by Buda et al.[16]

The presence of chelating nitrogen-donor ligands such as the bispidones, L^1 and L^2, will clearly alter the electron density at the metal centre relative to the aqua complex. Perhaps more significantly, the pentadentate nature of the ligand means that the coordination of additional water molecules is blocked in the putative intermediates, $[LFe^{II}(H_2O_2)]^{2+}$, and the all-important trapping of the developing OH radical in the first coordination sphere (Scheme 2) is therefore not possible. Nevertheless, Que and co-workers have shown that, in the case of $[(N4Py)Fe^{II}(CH_3CN)]^{2+}$, the addition of precisely 0.5 equiv. of H_2O_2 still gives quantitative oxidation to Fe^{III} {present as a mixture of $[(N4Py)Fe^{III}(OH)]^{2+}$ and the oxido-bridged dimer, $[(N4Py)Fe^{III}(O)Fe^{III}(N4Py)]^{4+}$} with no evidence of ligand oxidation.[4] Girerd and co-workers have observed similar behaviour in the reaction of Fe^{II} complexes of the trispicene ligand with H_2O_2, where the intermediate was tentatively assigned as $[LFe^{III}Cl]^{2+}$.[5c] From a mechanistic perspective, the clean oxidation of Fe^{II} to Fe^{III} with 0.5 equiv. of H_2O_2 seems inconsistent with the generation of free OH radicals, which would cause ligand degradation and therefore reduce the yield of Fe^{III}. The direct formation of transient $Fe^{IV}(O)$, followed by comproportionation with excess Fe^{II}, as proposed by Kremer, seems more consistent with this observation. Very recently, Comba and co-workers have studied the formation of $[L^2Fe^{IV}(O)]^{2+}$ from a mixture of the bispidone complex $[L^2Fe^{II}(BF_4)_2]$ and H_2O_2.[6c] The presence of clear isosbestic points in the UV/Vis spectrum, along with second-order kinetics and a large negative entropy of activation support a mechanism where binding of H_2O_2 to the Fe^{II} centre is followed by direct conversion to $Fe^{IV}(O)$ by O–O bond heterolysis. This pathway is quite different from the O–O bond *homolysis* proposed for the aqua complex,[16] and poses a number of intriguing questions regarding the precise role of the pentadentate ligand in the reaction.

In this paper, we use density functional theory to explore possible pathways that can lead to a high-valent $[LFe^{IV}(O)]^{2+}$ species from $[LFe^{II}(H_2O_2)]^{2+}$, where L is a member of the bispidone family. Specifically, we focus on the bispidone ligand L^1 shown in Scheme 1 above – a comparison of the properties of complexes of L^1 and L^2 will form the basis of a subsequent communication. In all cases, the ester groups on the ligand backbone have been replaced by hydrogen atoms to simplify the computational model. We identify two distinct mechanisms for decomposition of the hydrogen peroxide. The first is qualitatively similar to the homolytic fission pathway proposed for the aqua complex,[16] except in this case the developing OH radical is trapped in the vicinity of the metal centre only by non-covalent interactions. The second pathway, in contrast, involves proton transfer, mediated by a water molecule in the second coordination sphere, followed by heterolysis of the O–O bond, and so is very similar to the mechanism proposed in ref.[6b] The barriers to the two processes prove to be comparable, suggesting that subtle changes in ligand structure and/or reaction conditions could shift the balance from one to the other.

Results and Discussion

In the initial section, we present a detailed description of the electronic structure of the aqua complex, $[L^1Fe^{II}(H_2O)]^{2+}$, which we take as the starting point for these calculations, along with the various metal-based species that may play a role in the decomposition of H_2O_2: viz. the hydrogen peroxide adduct, $[L^1Fe^{II}(H_2O_2)]^{2+}$, the Fe^{III} intermediate, $[L^1Fe^{III}(OH)]^{2+}$ and the product $[L^1Fe^{IV}(O)]^{2+}$. We subsequently consider mechanisms for their interconversion, paying particular attention to the possible role of solvent.

Electronic Structure of $[L^1Fe^{II}(H_2O)]^{2+}$, $[L^1Fe^{II}(H_2O_2)]^{2+}$, $[L^1Fe^{III}(OH)]^{2+}$ and $[L^1Fe^{IV}(O)]^{2+}$

The optimised structures of the most stable spin states of $[L^1Fe^{II}(H_2O)]^{2+}$, $[L^1Fe^{II}(H_2O_2)]^{2+}$, $[L^1Fe^{III}(OH)]^{2+}$ and $[L^1Fe^{IV}(O)]^{2+}$ are shown in Figure 1, and the structural parameters for all accessible spin states are collected in Table 1. For both the aqua and hydrogen peroxide complexes, the optimised $S = 0$ and $S = 2$ structures show the typical features of low-spin/high-spin Fe^{II} species, with the metal–ligand bonds approximately 0.2 Å longer in the latter. A strong Jahn–Teller distortion is present in the triplet state, resulting in very long bonds to the H_2O and H_2O_2 ligands. The O–O bond in the hydrogen peroxide ligand is relatively insensitive to spin state, although the marginal elongation in the singlet can be ascribed to the better back-donating ability of low-spin Fe^{II}. The quintet is the most stable spin state in both systems, with relatively large gas-phase separations of ca. 35 kJ mol^{-1} to the singlet and ca. 45 kJ mol^{-1} to the intermediate spin[20] ($S = 1$) state. The inclusion of solvation through the PCM approach stabilises the $S = 0$ and, to a lesser extent, $S = 1$ states relative to the $S = 2$ ground state. The solvation energy in these systems is dominated by electrostatic interactions between the solvent continuum and the +2 charge on the solute, and its magnitude is therefore largely determined by the size of the solute cavity. The preferential stabilisation of states of lower multiplicity is therefore a general observation in these systems, and simply reflects the shorter Fe–N and Fe–O bonds, which lead in turn to a smaller solute cavity, and hence to stronger electrostatic interactions.

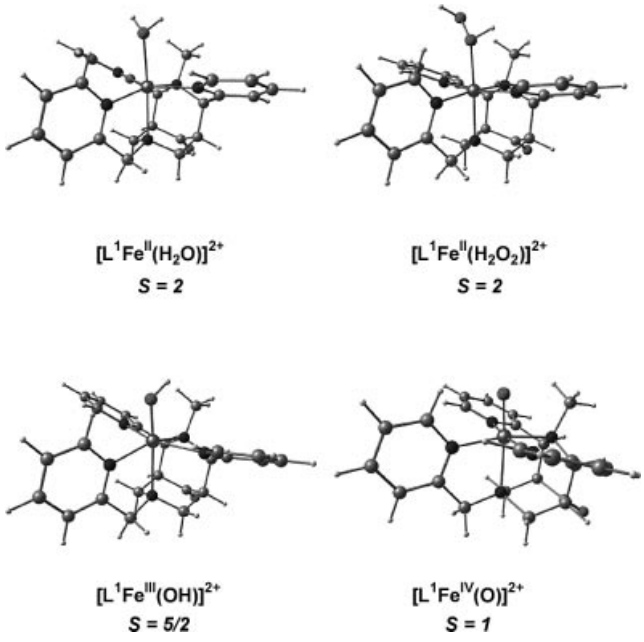

Figure 1. Optimised structures of the ground states of $[L^1Fe^{II}(H_2O)]^{2+}$, $[L^1Fe^{II}(H_2O_2)]^{2+}$, $[L^1Fe^{III}(OH)]^{2+}$ and $[L^1Fe^{IV}(O)]^{2+}$.

For the Fe^{III} intermediate, $[L^1Fe^{III}(OH)]^{2+}$, we have located distinct minima for $S = 1/2$, 3/2 and 5/2 spin states. The structures show the usual trend towards longer bonds in the higher multiplicity states, most obviously in the comparison of the equatorial Fe–N distances in the $S = 1/2$ and S = 5/2 states. In the gas phase, the sextet (shown in Figure 1c) is the most stable, but the doublet is only 8 kJ mol^{-1} higher in energy. We have noted above the tendency of solvation to stabilise lower spin states, and in this case it leads to a reversal of the order, with $S = 1/2$ lying 10 kJ mol^{-1} *below* $S = 5/2$. There has been considerable debate over the ability of density functional theory to accurately model spin-state splittings, and the case of Fe^{III} seems to be particularly problematic.[21] This uncertainty, along with the approximate nature of the PCM solvation model, precludes a definitive conclusion on the multiplicity of the ground state of $[L^1Fe^{III}(OH)]^{2+}$. Neither $[L^1Fe^{III}(OH)]^{2+}$ nor $[L^1Fe^{III}(Cl)]^{2+}$ has been isolated experimentally, although the hydroperoxide complex, $[L^1Fe^{III}(OOH)]^{2+}$, is known to have a doublet ground state.

The d^4 configuration of the $[L^1Fe^{IV}(O)]^{2+}$ species leads to $S = 0$, 1 and 2 spin states. Of these, the ground state (Figure 1, d) is clearly the triplet (gas phase and in solution), a situation typical of d^4 metal–oxido species, where two of the three t_{2g}-based orbitals are strongly destabilised by M–O π*-interactions. The open-shell singlet state ($<S^2> = 1.03$) has almost identical bond lengths and angles, and lies 38 kJ mol^{-1} higher in energy. High-spin states of $Fe^{IV}(O)$ have attracted considerable attention since the identification of such a species in the active site of the enzyme tauD,[3] but in this case the quintet lies 20 kJ mol^{-1} above the ground state, sufficient to rule out its participation in the oxidation pathway.

Table 1. Optimised Fe–N and Fe–O bond lengths [Å] and relative energies [kJ mol^{-1}] of the various spin states of $[L^1Fe^{II}(H_2O)]^{2+}$, $[L^1Fe^{II}(H_2O_2)]^{2+}$, $[L^1Fe^{III}(OH)]^{2+}$ and $[L^1Fe^{IV}(O)]^{2+}$. Energies are given relative to the most stable spin state for each species.

	$[L^1Fe^{II}(H_2O)]^{2+}$			$[L^1Fe^{II}(H_2O_2)]^{2+}$			$[L^1Fe^{III}(OH)]^{2+}$			$[L^1Fe^{IV}(O)]^{2+}$		
S	0	1	2	0	1	2	1/2	3/2	5/2	0	1	2
Fe–O	2.08	2.73	2.24	2.05	3.40	2.22	1.79	1.83	1.80	1.62	1.62	1.61
Fe–N^1	2.10	2.33	2.29	2.11	2.19	2.32	2.16	2.52	2.41	2.24	2.24	2.22
Fe–N^2	2.03	2.00	2.23	2.03	2.00	2.23	2.01	2.06	2.22	2.01	2.01	2.20
Fe–N^3	1.99	2.04	2.18	1.99	2.03	2.18	1.99	1.98	2.17	2.00	2.00	2.13
Fe–N^4	1.99	1.98	2.14	2.00	1.96	2.16	2.00	2.09	2.12	1.99	1.99	2.06
Fe–N^5	2.00	2.04	2.21	2.00	2.04	2.16	2.02	1.99	2.18	2.01	2.01	2.18
O–O				1.46	1.45	1.46						
$E_{(gas\text{-}phase)}$	+35	+50	0	+33	+40	0	+8	+55	0	+38	0	+20
$E_{(PCM)}$	+10	+38	0	+15	+33	0	0	+50	+12	+38	0	+32

Thermodynamics of the Decomposition of $[L^1Fe^{II}(H_2O_2)]^{2+}$ into $[L^1Fe^{IV}(O)]^{2+}$

The balanced equation for the decomposition of $[L^1Fe^{II}(H_2O_2)]^{2+}$ to $[L^1Fe^{IV}(O)]^{2+}$ via the putative $[L^1Fe^{III}(OH)]^{2+}$ intermediate is:

$$[L^1Fe^{II}(H_2O_2)]^{2+} \rightarrow [L^1Fe^{III}(OH)]^{2+} + OH \rightarrow [L^1Fe^{IV}(O)]^{2+} + H_2O$$

The first step, the homolytic cleavage of the O–O bond, is strongly endothermic [$\Delta E_{(gas\text{-}phase)} = +34\ kJ\,mol^{-1}$], while the second is highly exothermic [$\Delta E_{(gas\text{-}phase)} = -114\ kJ\,mol^{-1}$], and as a result the decomposition of $[(H_2O)_5Fe^{II}(H_2O_2)]^{2+}$ to $[L^2Fe^{IV}(O)]^{2+} + H_2O$ is strongly favoured [$\Delta E_{(gas\text{-}phase)} = -80\ kJ\,mol^{-1}$]. On purely thermodynamic grounds, therefore, the direct generation of Fe^{III}, along with the liberation of free OH radicals, seems rather unlikely. The alternative pathway to Fe^{III}, by comproportionation of $Fe^{IV}(O)$ with excess Fe^{II} is, in contrast, exothermic [$\Delta E_{(gas\text{-}phase)} = -62\ kJ\,mol^{-1}$], confirming it as the more likely source of Fe^{III} in this case:

$$[L^1Fe^{II}(H_2O)]^{2+} + [L^1Fe^{IV}(O)]^{2+} \rightarrow 2\,[L^1Fe^{III}(OH)]^{2+}$$

Influence of Solvent

When considering possible pathways that might link the various species discussed in the previous section, we need to pay careful attention to the motion of hydrogen atoms as well as the cleavage of the O–O bond. Indeed, the role of a water ligand as a hydrogen-atom shuttle has been highlighted previously.[16] We have noted above that water is excluded from the first coordination sphere by the pentadentate bispidone ligand, and so for the exploration of reaction pathways we choose the solvated species $[L^1Fe^{II}(H_2O_2)]^{2+}\cdot H_2O$ as our minimal model, where the second coordination sphere water can, at least in principle, play the same role as the water ligand in $[(H_2O)_5Fe^{II}(H_2O_2)]^{2+}$. The balanced equation for the decomposition of the H_2O_2 complex is then:

$$[L^1Fe^{II}(H_2O_2)]^{2+}\cdot H_2O \rightarrow [L^1Fe^{III}(OH)]^{2+}\cdot H_2O\cdot OH \rightarrow [L^1Fe^{IV}(O)]^{2+}\cdot 2H_2O$$

Representative structures of the important hydrated species are shown in Figure 2, and the optimised energies and bond lengths are collected in Table 2. The oxygen and hydrogen atoms on the hydrogen peroxide are labelled as proximal (p) and terminal (t), while those on the water molecule are labelled "w" (see Figure 2, inset, for a schematic diagram of the hydrogen-bonded network). In the hydrogen peroxide complexes ($S = 0$, 1 and 2), the water molecule is aligned such that one lone pair interacts with the more acidic proton on the proximal (coordinated) oxygen centre. A comparison of Table 1 and Table 2 confirms that the additional water molecule has only a marginal impact on the metal–ligand bond lengths and the relative stabilities of the different spin states. The only exception is the highly distorted $S = 1$ state, where the increased basicity of the proximal oxygen atom on the H_2O_2 ligand results in a significant contraction of the Fe–O and Fe–N^2 bonds.

We have identified minima corresponding to the caged radical species $[L^1Fe^{III}(OH)]^{2+}\cdot H_2O\cdot OH$ in four distinct spin states ($S = 0$, 1, 2 and 3). The optimised structure of the most stable gas-phase species ($S = 2$) is shown in Fig-

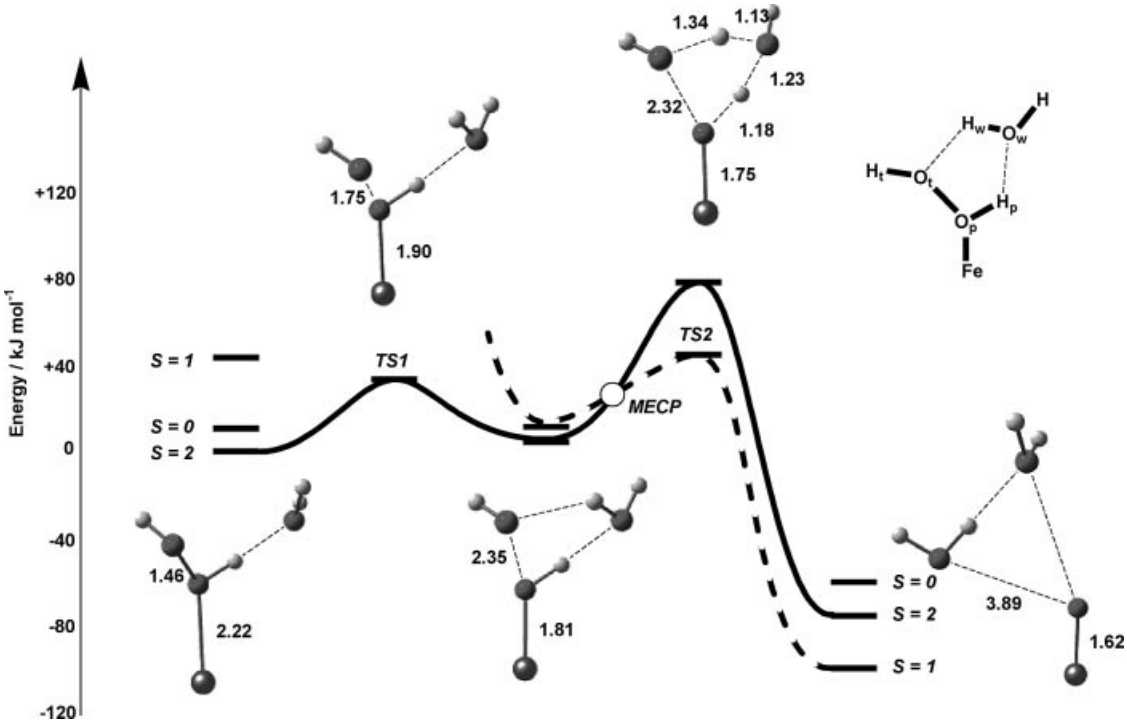

Figure 2. Potential energy surface for the O–O homolysis pathway for decomposition of $[L^1Fe^{II}(H_2O_2)]^{2+}\cdot H_2O$. Energies include the effects of solvation introduced by the PCM model. For clarity, the bispidone ligand is not shown in the structures.

Table 2. Optimised Fe–N and Fe–O bond lengths [Å] and relative energies [kJ mol^{-1}] for stationary points on the O–O homolysis pathway linking $[L^1Fe^{II}(H_2O_2)]^{2+}\cdot H_2O$ and $[L^1Fe^{IV}(O)]^{2+}\cdot 2H_2O$. Energies of all species are reported relative to the S = 2 ground state of the $[L^1Fe^{II}(H_2O_2)]^{2+}\cdot H_2O$ complex.

	$[L^1Fe^{II}(H_2O_2)]^{2+}\cdot H_2O$			$[L^1Fe^{III}(OH)]^{2+}\cdot H_2O\cdot OH$				$[L^1Fe^{IV}(O)]^{2+}\cdot 2H_2O$			**TS1**	MECP	**TS2**		**TS3**		
S	0	1	2	0	1	2	3	0	1	2	2	1, 2	1	2	0	1	2
Fe–O	2.05	2.34	2.22	1.79	1.79	1.81	1.81	1.62	1.62	1.61	1.90	1.78	1.75	1.73	1.96	2.02	1.98
Fe–N^1	2.11	2.37	2.32	2.18	2.18	2.43	2.45	2.25	2.25	2.22	2.37	2.19	2.20	2.20	2.13	2.47	2.37
Fe–N^2	2.03	2.03	2.23	2.01	2.01	2.21	2.22	2.00	2.01	2.20	2.21	2.17	2.01	2.23	2.03	2.07	2.24
Fe–N^3	1.99	1.99	2.18	2.01	2.00	2.15	2.15	2.01	2.00	2.12	2.16	2.06	1.98	2.08	2.01	1.98	2.21
Fe–N^4	2.00	2.04	2.16	2.01	2.00	2.13	2.13	1.99	1.99	2.06	2.14	2.11	2.01	2.11	2.00	2.09	2.17
Fe–N^5	2.00	1.99	2.16	1.99	2.00	2.18	2.18	2.01	2.01	2.21	2.22	2.09	2.02	2.16	1.99	1.99	2.23
O_p–O_t	1.46	1.46	1.46	2.32	2.53	2.35	2.60	3.89	3.89	3.63	1.75	2.52	2.32	2.36	1.52	1.52	1.54
O_p–H_p	1.00	1.00	1.00	0.99	1.00	0.99	0.99	6.37	6.37	6.71	1.00	0.99	1.18	1.20	1.73	1.74	1.72
H_p–O_w	1.66	1.68	1.66	1.73	1.72	1.81	1.80	0.97	0.97	0.97	1.66	1.79	1.23	1.22	1.02	1.02	1.02
O_w–H_w	0.97	0.97	0.97	0.98	0.98	0.98	0.98	1.85	1.85	1.80	0.97	0.98	1.13	1.11	1.11	1.11	1.11
H_w–O_t	3.07	3.04	3.19	1.98	1.95	1.98	1.95	0.98	0.98	0.99	2.26	1.93	1.34	1.36	1.38	1.37	1.38
$E_{(gas\text{-}phase)}$	31	50	0	20	27	11	16	–61	–99	–78	40	57	79	104	130	156	101
$E_{(PCM)}$	13	44	0	1	8	3	8	–63	–101	–80	34	23	44	78	101	133	87

ure 2, and bond lengths for all four spin states are collected in Table 2. The complex spin-state manifold in this region of the potential energy surface arises from parallel (ferromagnetic) or antiparallel (antiferromagnetic) alignment of the spins on the $[L^1Fe^{III}(OH)]^{2+}$ (S = 1/2, 3/2, 5/2) and OH radicals (S = 1/2), giving rise to coupled spin states with total S = 0, 1, 2 and 3. The description of the S = 3 spin state is unambiguous – it can only be achieved through parallel alignment of the spin vectors on S = 5/2 Fe^{III} and S = 1/2 OH, and indeed the structural parameters and net spin densities (4.22 on Fe, 0.94 on O_t) confirm this to be the case. Likewise, the S = 0 state arises unambiguously from the antiparallel alignment of S = 1/2 Fe^{III} and S = 1/2 OH (net spin densities 0.95 on Fe, –0.93 on O_t). In contrast, the S = 1 and S = 2 states could, in principle, contain intermediate spin (S = 3/2) Fe^{III}. However, the rather high energy of this spin state in isolated $[L^1Fe^{III}(OH)]^{2+}$ (Table 1) suggests that this is unlikely, and indeed the Fe–N and Fe–O bond lengths in the S = 1 and S = 2 states are almost identical to those in S = 0 and S = 3, confirming the presence of low- and high-spin Fe^{III}, respectively. When the alignment of spins is antiparallel (S = 0, 2), the separation between proximal oxygen atom (O_p) and the hydroxyl radical (O_t) is somewhat smaller than where the alignment is parallel (S = 1, 3), but the rather small energy differences between S = 0 and 1 (7 kJ mol^{-1}) and between S = 2 and 3 (5 kJ mol^{-1}) are indicative of only weak coupling.

The most stable spin state (S = 2 in the gas phase) lies only 11 kJ mol^{-1} above the reactants, representing a substantial stabilisation relative to the fully separated reactants, $[L^1Fe^{III}(OH)]^{2+}$ and OH (ΔE = +34 kJ mol^{-1}). The much lower energy required to cleave the O–O bond is due to the residual electrostatic attraction between the OH radical and the +2 cation in the "caged radical" species, $[L^1Fe^{III}(OH)]^{2+}\cdot H_2O\cdot OH$, that is absent in the separated species. As was the case for the isolated $[L^1Fe^{III}(OH)]^{2+}$ molecule, solvation (introduced through the PCM model) has a significant impact on the manifold of spin states, selectively stabilising those containing the smaller low-spin Fe^{III} centre (S = 0, 1) relative to those containing high-spin Fe^{III} (S = 2, 3). As a result, the S = 0 state becomes the most stable at this level of theory, and the caged radical is now almost isoenergetic with the hydrogen peroxide complex. At this point, it is useful to contrast the pathway shown in Figure 2 with that described for $[(H_2O)_5Fe(H_2O_2)]^{2+}$.[16] In this aqua complex, the incipient OH radical is "trapped" by abstracting a hydrogen atom from a neighbouring water molecule, and the strength of the resultant Fe–OH bonds stabilises the intermediate, such that it lies over 80 kJ mol^{-1} below the hydrogen peroxide complex. In the case of $[L^1Fe^{II}(H_2O_2)]^{2+}$, the free OH radical is trapped only by electrostatic interactions with the +2 charge on the metal core, along with hydrogen bonding with the solvent cage, and as a result, the O–O homolysis step is less favourable (ΔE = 11 kJ mol^{-1}, in the gas phase and +1 kJ mol^{-1} at the PCM level of theory). In the context of the reaction chemistry, the weak trapping of the radical means that diffusion to neighbouring organic species may be competitive with a "rebound" reaction with the $Fe^{III}(OH)$ unit. Caged radicals such as these have previously been proposed to play a role in oxidation chemistry.[6b,22]

In the $[L^1Fe^{IV}(O)]^{2+}$ complex, the presence of the two additional water molecules has a negligible impact on either the relative energies of the spin states or on the bond lengths in the first coordination sphere. The interaction energy between the complex and the solvent molecules is again dominated by the electrostatic interaction with the +2 charge on the metal core, and so the presence of the additional water molecule stabilises the products by 19 kJ mol^{-1} relative to the hydrogen peroxide complex.

In terms of the overall energetics of the reaction, the picture is largely unaffected when we consider the "supermolecule" $[L^1Fe^{II}(H_2O_2)]^{2+}\cdot H_2O$ rather than the fully separated species The intermediate and products are stabilised by electrostatic interactions between the dicationic core and the OH or H_2O unit that is generated by cleavage of the O–O bond, but this serves only to increase the already substantial thermodynamic driving force for the cleavage of the O–O bond. It is also important to note that the mixture of explicit and continuum models for solvent described above

is problematic, particularly where a solvent molecule is involved in the reaction[23] {in our case one molecule of H_2O is formed in the reaction $[L^1Fe^{II}(H_2O_2)]^{2+}\cdot H_2O \rightarrow [L^1Fe^{IV}(O)]^{2+}\cdot 2H_2O$}. In the context of this work, the non-cancellation of errors that arises through the mixture of continuum and explicit solvent models introduces significant uncertainties in the accuracy of the computed energies of the different asymptotes. In the remainder of this paper, we therefore focus on the qualitative mechanistic picture, and do not place undue emphasis on the absolute values of the computed energies.

In the following sections we describe two distinct pathways that lead to the formation of an $Fe^{IV}(O)$ species – the first where O–O bond homolysis is followed by hydrogen-atom abstraction, the second where proton transfer induces O–O bond heterolysis. In both cases, we pay particular attention to the various spin states that are accessible at different points on the potential energy surface. This latter point is critical here because the ground states of the $[L^1Fe^{II}(H_2O_2)]^{2+}$ and $[L^1Fe^{IV}(O)]^{2+}$ species are a quintet and a triplet, respectively. Intersystem crossing from one potential energy surface to the other is therefore an integral component of the reaction coordinate.

O–O Bond Homolysis Pathway

We have located a transition state, **TS1**, linking the reactant, $[L^1Fe^{II}(H_2O_2)]^{2+}\cdot H_2O$, and the caged radical, $[L^1Fe^{III}(OH)]^{2+}\cdot H_2O\cdot OH$, on the $S = 2$ surface. The O–O bond is significantly elongated at the transition structure (1.75 Å vs. 1.46 Å in the reactants), and the imaginary frequency is clearly associated with the O–O stretching mode. The Fe–O separation is also significantly reduced compared to the reactants, due to the partial oxidation of the metal centre. We have also located transition states (**TS2**) linking the radical intermediates with the $[L^1Fe^{IV}(O)]^{2+}\cdot 2H_2O$ asymptote on both quintet and triplet surfaces. At this point, the O_p–H_p distance is significantly elongated while the separation between this hydrogen atom and the OH radical is much reduced, and the imaginary frequency corresponds to an O_p–H_p stretch. The net effect is that the solvent water molecule acts as a hydrogen atom shuttle, mediating the abstraction of a hydrogen atom from the coordinated OH ligand by the OH radical. The energy of **TS2** is highly dependent on the spin state – the triplet lies significantly *below* the quintet, reflecting its product-like nature. The shape of the potential energy surfaces also dictates that the crossover between the quintet and triplet surfaces must occur at some point between the radical intermediate ($S = 2$) and **TS2** ($S = 1$). We have located the minimum energy crossing point (MECP1) between these surfaces, and the structural changes leading up to this point are largely associated with the metal–ligand bonds, all of which contract significantly from the intermediate to the MECP. The separation between the metal fragment and the OH radical is, in contrast, essentially unchanged. We therefore conclude that the crossover from the quintet to triplet surfaces involves a localised $S = 5/2 \rightarrow S = 1/2$ transition on the Fe^{III} centre, and the nature of the interaction between the metal centre and the OH radical remains unchanged. In the gas phase, the MECP lies 46 kJ mol^{-1} above the $S = 2$ intermediate, but this is reduced to 31 kJ mol^{-1} when solvation is included, as a result of the contracted metal–ligand bonds in the former. It is important to emphasise, however, that the effects of solvation are only included post-optimisation. We have noted previously that solvation stabilises low-spin states, and indeed the $S = 1$ and $S = 2$ caged radical species are almost isoenergetic when solvation effects are included. If the energies of these two states were, in fact, reversed, then the $S = 2 \rightarrow S = 1$ spin crossover would occur before, rather than just after, the radical intermediate. Given the intrinsic uncertainties in determining accurate spin-state energies with DFT and the approximate nature of the PCM solvation model, we are unable to reach a definitive conclusion on this point. It will not, however, have a major impact on the potential energy surface: the nature of the crossover – viz. a localised high-spin/low-spin transition on the Fe^{III} centre – remains unchanged.

To summarise, the early part of the reaction coordinate shown in Figure 2 lies along the quintet surface, and involves homolysis of the O–O bond. The resulting intermediate contains an $[L^1Fe^{III}(OH)]^{2+}$ species, weakly coupled to an OH radical, the whole unit being held together by electrostatic interactions with the dicationic metal core and hydrogen bonding within the solvent cage. A localised high-spin/low-spin transition on the Fe^{III} centre then causes a crossover to the triplet surface, after which the OH radical abstracts a hydrogen atom from the coordinated OH ligand. Whilst the initial O–O bond homolysis step was marginally endothermic, the hydrogen atom abstraction step is highly exothermic, and the $[L^1Fe^{IV}(O)]^{2+}$ product is 101 kJ mol^{-1} more stable than the reactants. In comparison, a value of 117 kJ mol^{-1} was reported for the aqua complex.[16] Thus, the major difference between the two pathways lies not in the overall exothermicity of the decomposition of the H_2O_2 complex, but rather in the details of the intervening potential energy surface. In the aqua complex, the O–O homolysis and hydrogen atom abstraction steps are concerted, while in the case of $[L^1Fe^{II}(H_2O_2)]^{2+}$, the absence of an additional water ligand effectively separates the two processes, leading to an identifiable $Fe^{III}(OH)$ intermediate. The rate-determining step in this reaction clearly depends on the relative energies of the two transition states, **TS1** and **TS2** shown in Figure 2. In the gas phase, **TS2** (79 kJ mol^{-1}) lies substantially above **TS1** (40 kJ mol^{-1}), suggesting that the OH "rebound" step should be rate-determining. In these circumstances, diffusion of the OH radical into solution should be competitive with formation of the $Fe^{IV}(O)$ species. However, when solvation is included, **TS2** is strongly stabilised relative to **TS1** because the latter contains the smaller low-spin Fe^{III} centre, and the two barriers are now rather similar (34 and 44 kJ mol^{-1}, respectively). We return to a discussion of this point in the concluding remarks.

O–O Bond Heterolysis Pathway

In the previous section we identified a pathway linking the two asymptotes, $[L^1Fe^{II}(H_2O_2)]^{2+}\cdot H_2O$ and $[L^1Fe^{IV}(O)]^{2+}\cdot 2H_2O$, via an intermediate containing a weakly trapped OH radical. Comba, Que and co-workers have proposed an alternative pathway involving proton (as distinct from hydrogen atom) transfer, followed by O–O heterolysis, to account for the observed decomposition of $[L^2Fe^{II}(H_2O_2)]^{2+}$.[6c] We have considered this possibility, and identified a further transition state, **TS3**, that directly links the reactants and products for each of the three spin states (S = 0, 1, 2). The structure of the most stable transition state (S = 2) is shown in Figure 3, and key bond lengths for all three are collected in Table 2. The most remarkable feature of the transition structures is the near-identical geometry of the $H_2O_2\cdot H_2O$ unit in each case. The proton initially attached to the proximal oxygen atom of the hydrogen peroxide has been almost completely transferred to the water molecule ($O_p\cdots H_p$ = 1.72–1.74 Å, H_p–O_w = 1.02 Å), suggesting that the reaction coordinate leading up to the transition state is a simple proton transfer. The Fe–O bond lengths contract somewhat as a result of the removal of the proximal proton (by 0.24 Å for S = 2), but the equatorial and axial Fe–N distances remain largely unchanged. The marginal elongation of the O–O bond (1.52–1.54 Å, c.f. 1.45–1.46 in the equilibrium structures) also confirms that O–O bond cleavage is not well advanced at the transition state. The imaginary frequency in each spin state corresponds to the transfer of the proton from H_3O^+ to the terminal oxygen atom of the hydrogen peroxide, and a small displacement along this mode results in decomposition to the hydrated $[L^1Fe^{IV}(O)]^{2+}\cdot 2H_2O$ species, with no further barrier. Given that the motion along the reaction coordinate prior to the transition state is almost entirely centred on the $H_2O_2\cdot H_2O$ unit, it is unsurprising that the barriers, measured relative to the reactant, are essentially independent of the spin state of the iron centre (87–89 kJ mol^{-1}, Figure 3). The lowest energy pathway therefore lies along the quintet surface until well after the transition state. Intersystem crossing between the S = 2 and S = 1 surfaces must again occur at some later stage on the reaction coordinate, and will correspond to a localised high-spin/low-spin transition on the developing $Fe^{IV}(O)$ unit. In summary, although the proton-transfer mechanism leading to O–O bond cleavage is concerted and does not involve any stable intermediates, it is also highly asynchronous. The reaction coordinate prior to the transition state involves deprotonation of the hydrogen peroxide ligand at the proximal oxygen atom, while afterwards transfer of the proton to the terminal oxygen leads to spontaneous cleavage of the O–O bond. This mechanism is qualitatively similar to that proposed by Que and Comba for the decomposition of $[L^2Fe^{IV}(H_2O_2)]^{2+}$, with the subtle difference that it is the proton transfer, rather than the O–O bond heterolysis, that determines the magnitude of the barrier.

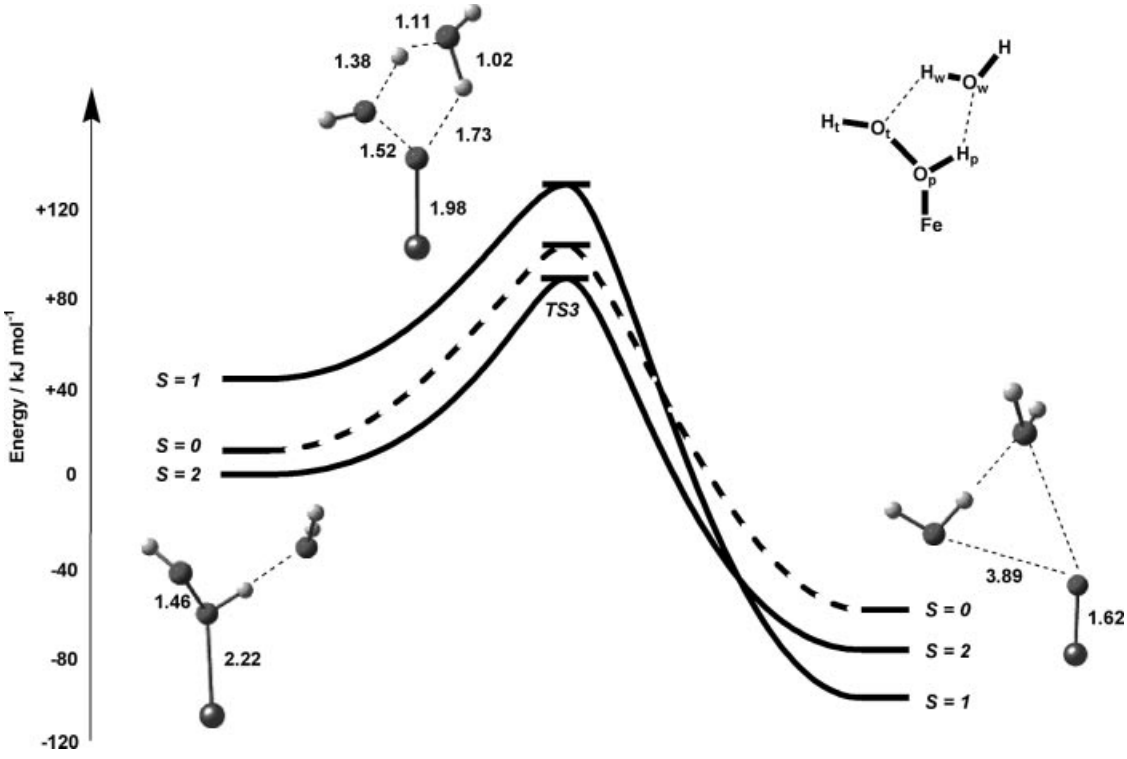

Figure 3. Potential energy surface for the O–O bond heterolysis mechanism for decomposition of $[L^1Fe^{II}(H_2O_2)]^{2+}\cdot H_2O$. Energies include the effects of solvation introduced by the PCM model.

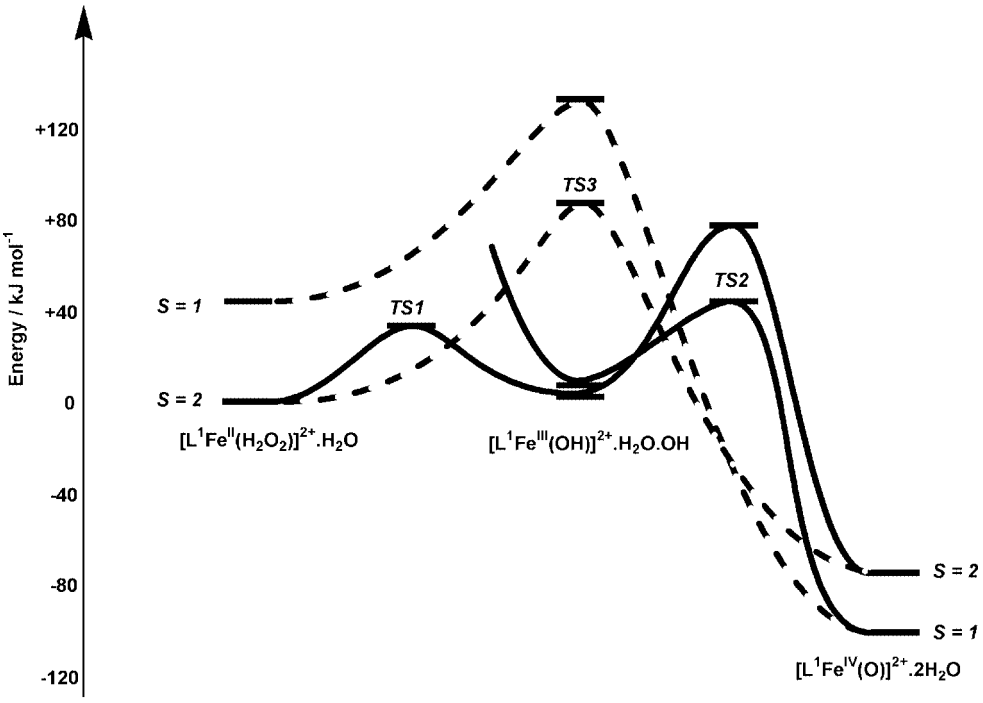

Figure 4. Comparison of the key features of the potential energy surface homolytic and heterolytic (dashed) O–O bond cleavage in $[L^1Fe^{II}(H_2O_2)]^{2+}\cdot H_2O$.

Conclusions

The key features of the two possible pathways for O–O bond cleavage are compared in Figure 4. Returning to the question of radical (Haber–Weiss) vs. non-radical (Bray–Gorin) mechanisms, we can identify three quite distinct scenarios, depending on the relative energies of the three transition states **TS1**, **TS2** and **TS3**. If **TS3** < **TS1**, the concerted mechanism will dominate, and any Fe^{III} product must be generated by comproportionation of the initially formed $Fe^{IV}(O)$ with excess Fe^{II}. If, in contrast, **TS3** > **TS1**, then the homolytic pathway will dominate, and this in turn can lead to two distinct outcomes depending on the energies of **TS1** and **TS2**. If **TS1** > **TS2**, rebound of the transient OH radical will be rapid, leading again to formation of $Fe^{IV}(O)$, but in this case via transient $Fe^{III}(OH)$. In contrast, if **TS2** > **TS1**, the products of the reaction will depend critically on the rate of the rebound step (**TS2**) relative to the rate of diffusion through the solvent. If the latter is rapid, then the OH radicals are likely to escape and oxidise the ligand, solvent or any other accessible substrate. The presence of three distinct scenarios offers a possible explanation for the very complex nature of Fenton chemistry, and in particular for the apparent generation of radicals in some cases but not others.[11] It also provides a framework for understanding the way in which changes in ligand can perturb the reaction pathway.

Calculation Details

In all cases, the bispidone ligand was simplified by replacing the ester groups with hydrogen atoms. All calculations described in this paper were performed using the Gaussian03 package.[24] The B3LYP[25b,25c] functional was used throughout, in conjunction with the 6-31G* basis set on all atoms. Full geometry optimisations were performed without symmetry constraints, and stationary points were characterised as minima or transition states by vibrational analysis. Minimum energy crossing points (MECPs) were located using the code developed by Harvey and co-workers.[26] Solvation energies were calculated by Tomasi's reaction field method using the polarized continuum model (PCM) with a dielectric constant (ε) of 78.39.

Acknowledgments

A. A. acknowledges financial support from the EPSRC and Unilever Research.

[1] a) E. I. Solomon, *Inorg. Chem.* **2001**, *40*, 3656; b) E. I. Solomon, T. C. Brunold, M. I. Davis, J. N. Kemsley, S.-K. Lee, N. Lehnert, F. Neese, A. J. Skulan, Y.-S. Yang, J. Zhou, *Chem. Rev.* **2000**, *100*, 235.

[2] a) N. Lehnert, F. Neese, R. Y. N. Ho, L. Que Jr, E. I. Solomon, *J. Am. Chem. Soc.* **2002**, *124*, 10810; b) F. Neese, J. M. Zaleski, K. Loeb Zaleski, E. I. Solomon, *J. Am. Chem. Soc.* **2000**, *122*, 11703.

[3] P. J. Riggs-Gelasco, J. C. Price, R. B. Guyer, J. J. Brehm, E. W. Barr, J. M. Bollinger Jr, C. Krebs, *J. Am. Chem. Soc.* **2004**, *126*, 8108.

[4] a) M. Lubben, A. Meetsma, E. C. Wilkinson, B. L. Feringa, L. Que Jr, *Angew. Chem. Int. Ed. Engl.* **1995**, *34*, 1512; b) G. Roelfes, M. Lubben, K. Chen, R. Y. N. Ho, A. Meetsma, S. Genseberger, R. H. Hermant, R. Hage, S. K. Mandal, V. G. Young Jr, Y. Zang, H. Kooijman, A. L. Spek, L. Que Jr, B. L. Feringa, *Inorg. Chem.* **1999**, *38*, 1929; c) R. Y. N. Ho, G. Roelfes, B. L. Feringa, L. Que Jr, *J. Am. Chem. Soc.* **1994**, *116*, 264; d) G. Roelfes, M. Lubben, R. Hage, L. Que Jr, B. L. Feringa, *Chem. Eur. J.* **2000**, *6*, 2152.

[5] a) I. Bernal, I. M. Jensen, K. B. Jensen, C. J. McKenzie, H. Toftlund, J. P. Tuchagues, *J. Chem. Soc., Dalton Trans.* **1995**, 3667; b) V. Balland, F. Banse, E. Anxolabehere-Mallart, M. Ghiladi, T. A. Mattioli, C. Pilouze, G. Blondin, J.-J. Girerd, *Inorg. Chem.* **2003**, *42*, 2470; c) P. Mialane, A. Novorojkine, G. Pratviel, L. Azema, M. Slany, F. Godde, A. J. Simaan, F. Banse, T. Kargar-Grisel, G. Bouchoux, J. Saiton, O. Horner, J. Guilheim, L. Tchertanov, B. Meunier, J.-J. Girerd, *Inorg. Chem.* **1999**, *38*, 1085.

[6] a) M. R. Bukowksi, P. Comba, C. Limberg, M. Merz, L. Que Jr, T. Wistuba, *Angew. Chem. Int. Ed.* **2004**, *43*, 1283; b) M. R. Bukowski, P. Comba, A. Lienke, C. Limberg, C. Lopez de Laorden, R. Mas-Balleste, M. Merz, L. Que Jr, *Angew. Chem. Int. Ed.* **2006**, *45*, 3446; c) J. Bautz, M. R. Bukowski, M. Kerscher, A. Stubna, P. Comba, A. Lienke, E. Muenck, L Que Jr, *Angew. Chem*., in press; d) J. Bautz, P. Comba, L. Que Jr, *Inorg. Chem*., accepted.

[7] R. Hage, A. Lienke, *Angew. Chem. Int. Ed.* **2006**, *45*, 2006.

[8] A. Hazel, C. J. McKenzie, L. P. Nielsen, S. Schindler, M. Weitzer, *J. Chem. Soc., Dalton Trans.* **2002**, 310.

[9] a) N. Lehnert, R. Y. N. Ho, L. Que Jr, E. I. Solomon, *J. Am. Chem. Soc.* **2001**, *123*, 12802; b) A. Decker, M. S. Chow, J. N. Kemsley, N. Lehnert, E. I. Solomon, *J. Am. Chem. Soc.* **2006**, *128*, 4719.

[10] H. J. H. Fenton, *J. Chem. Soc.* **1894**, *65*, 889.

[11] a) D. T. Sawyer, A. Sobkowiak, T. Matsushita, *Acc. Chem. Res.* **1996**, *29*, 409; b) C. Walling, *Acc. Chem. Res.* **1998**, *31*, 155; c) P. H. MacFaul, D. D. M. Wayner, K. W. Ingold, *Acc. Chem. Res.* **1998**, *31*, 159; d) S. Goldstein, D. Meyerstein, *Acc. Chem. Res.* **1999**, *32*, 547.

[12] F. Haber, J. Weiss, *Proc. R. Soc. London* **1934**, *147*, 332.

[13] W. G. Barb, J. H. Baxendale, P. George, K. R. Hargrave, *Trans. Faraday Soc.* **1951**, *47*, 462.

[14] W. C. Bray, M. H. Gorin, *J. Am. Chem. Soc.* **1932**, *54*, 2124.

[15] M. L. Kremer, *Phys. Chem. Chem. Phys.* **1999**, *1*, 3595.

[16] F. Buda, B. Ensing, M. C. M. Gribnau, E. J. Baerends, *Chem. Eur. J.* **2001**, *7*, 2775.

[17] B. Ensing, F. Buda, P. Blöchl, E. J. Baerends, *Angew. Chem. Int. Ed.* **2001**, *113*, 2977.

[18] M. Masarwa, H. Cohen, D. Meyerstein, D. L. Hickman, A. Bakac, J. H. Espenson, *J. Am. Chem. Soc.* **1988**, *110*, 4293.

[19] a) O. Pestovsky, S. Stoian, E. L. Bominaar, X. Shan, E. Münck, L. Que Jr, A. Bakac, *Angew. Chem. Int. Ed.* **2005**, *44*, 6871; b) O. Pestovsky, A. Bakac, *J. Am. Chem. Soc.* **2004**, *126*, 15757.

[20] H. Keutel, I. Kapplinger, E.-G. Jager, M. Grodzicki, V. Schunemann, A. X. Trautwein, *Inorg. Chem.* **1999**, *38*, 2320.

[21] a) A. Ghosh, E. Tangen, H. Ryeng, P. R. Taylor, *Eur. J. Inorg. Chem.* **2004**, 4555; b) A. Ghosh, P. R. Taylor, *Curr. Opin. Chem. Biol.* **2003**, *7*, 113.

[22] Y. Mekmouche, S. Menage, C. Toia-Duboc, M. Fontecave, J.-B. Galey, C. Lebrun, J. Pecaut, *Angew. Chem. Int. Ed.* **2001**, *40*, 949.

[23] X. Fang, M.-H. Baik, *J. Am. Chem. Soc.* **2006**, *128*, 7476.

[24] M. J. Frisch, G. W. Trucks, H. B. Schlegel, G. E. Scuseria, M. A. Robb, J. R. Cheeseman, J. A. Montgomery Jr, T. Vreven, K. N. Kudin, J. C. Burant, J. M. Millam, S. S. Iyengar, J. Tomasi, V. Barone, B. Mennucci, M. Cossi, G. Scalmani, N. Rega, G. A. Petersson, H. Nakatsuji, M. Hada, M. Ehara, K. Toyota, R. Fukuda, J. Hasegawa, M. Ishida, T. Nakajima, Y. Honda, O. Kitao, H. Nakai, M. Klene, X. Li, J. E. Knox, H. P. Hratchian, J. B. Cross, C. Adamo, J. Jaramillo, R. Gomperts, R. E. Stratmann, O. Yazyev, A. J. Austin, R. Cammi, C. Pomelli, J. W. Ochterski, P. Y. Ayala, K. Morokuma, G. A. Voth, P. Salvador, J. J. Dannenberg, V. G. Zakrzewski, S. Dapprich, A. D. Daniels, M. C. Strain, O. Farkas, D. K. Malick, A. D. Rabuck, K. Raghavachari, J. B. Foresman, J. V. Ortiz, Q. Cui, A. G. Baboul, S. Clifford, J. Cioslowski, B. B. Stefanov, G. Liu, A. Liashenko, P. Piskorz, I. Komaromi, R. L. Martin, D. J. Fox, T. Keith, M. A. Al-Laham, C. Y. Peng, A. Nanayakkara, M. Challacombe, P. M. W. Gill, B. Johnson, W. Chen, M. W. Wong, C. Gonzalez, J. A. Pople, *Gaussian 03*, Revision B.03, Gaussian, Inc., Pittsburgh, PA, **2003**.

[25] a) A. D. Becke, *Phys. Rev. A* **1988**, *38*, 3098; b) A. D. Becke, *J. Chem. Phys.* **1993**, *98*, 1372; c) A. D. Becke, *J. Chem. Phys.* **1993**, *98*, 5648; d) S. H. Vosko, L. Wilk, M. Nusair, *Can. J. Phys.* **1980**, *58*, 1200; e) C. Lee, W. Yang, R. G. Parr, *Phys. Rev. B* **1988**, *37*, 785; f) A. D. Becke, *J. Chem. Phys.* **1986**, *84*, 4524; g) J. P. Perdew, *Phys. Rev. B* **1986**, *33*, 8822.

[26] a) J. N. Harvey, M. Aschi, H. Schwarz, W. Koch, *Theor. Chem. Acc.* **1998**, *99*, 95; b) J. N. Harvey, M. Aschi, *Phys. Chem. Chem. Phys.* **1999**, *1*, 5555.

Received: August 25, 2006
Published Online: November 17, 2006

